

# Energy & Environmental Science

Accepted Manuscript



This is an *Accepted Manuscript*, which has been through the Royal Society of Chemistry peer review process and has been accepted for publication.

*Accepted Manuscripts* are published online shortly after acceptance, before technical editing, formatting and proof reading. Using this free service, authors can make their results available to the community, in citable form, before we publish the edited article. We will replace this *Accepted Manuscript* with the edited and formatted *Advance Article* as soon as it is available.

You can find more information about *Accepted Manuscripts* in the [Information for Authors](#).

Please note that technical editing may introduce minor changes to the text and/or graphics, which may alter content. The journal's standard [Terms & Conditions](#) and the [Ethical guidelines](#) still apply. In no event shall the Royal Society of Chemistry be held responsible for any errors or omissions in this *Accepted Manuscript* or any consequences arising from the use of any information it contains.

# High efficiency stable inverted perovskite solar cells without current hysteresis

Chun-Guey Wu<sup>a,b,\*</sup>, Chien-Hung Chiang<sup>b</sup>, Zong-Liang Tseng<sup>b</sup>, Nazeeruddin Md. Khaja<sup>c,\*</sup>, Hagfeldt Anders<sup>c,\*</sup>, Michael Grätzel<sup>c,\*</sup>

<sup>a</sup>*Department of Chemistry, National Central University,*

<sup>b</sup>*Research Center for New Generation Photovoltaics, National Central University, Zhong-Li, 32001, Taiwan, ROC.*

<sup>c</sup>*Laboratory of Photonics and Interfaces, Swiss Federal Institute of Technology (EPFL), Station 6, Lausanne, CH 1015, Switzerland*

E-mail address of Professor C. G. Wu: [t610002@cc.ncu.edu.tw](mailto:t610002@cc.ncu.edu.tw)

**Abstract:**

The inverted perovskite solar cell fabricated with two-step method exhibited the highest FF of 0.85 and good efficiency of 18% based on  $\text{CH}_3\text{NH}_3\text{PbI}_3$ . A small amount of  $\text{H}_2\text{O}$  was added into  $\text{PbI}_2/\text{DMF}$  to make a homogenous precursor solution. High quality  $\text{PbI}_2$  film with full coverage was formed on PEDOT:PSS surface by spin coating of the homogeneous  $\text{PbI}_2$  precursor solution. Perovskite film fabricated from the high quality  $\text{PbI}_2$  film is highly pure, smooth and very dense even without any pinhole. The champion cell achieves a remarkable fill factor (FF) of 0.85, which is the highest value reported in perovskite solar cells. The FF value is also very reproducible with less than 10% deviation for 50 cells. The cell exhibits no current hysteresis and is stable under both dark and illumination in the dry and inert atmosphere. The results not only provide a strategy to fabricate high efficiency inverted perovskite solar cell but also reveal how water additive in  $\text{PbI}_2/\text{DMF}$  solution may affect the properties of  $\text{PbI}_2$  and therefore perovskite film prepared with two-step method and the overall photovoltaic performance of the corresponding inverted solar cell.

Photovoltaic device which converts Sun energy into electricity is one of the important technologies for the renewable energy. Photovoltaic cells using perovskite as photo absorber and carrier transporter is a burgeoning research, since perovskite based solar cells have not only the high power conversion efficiency<sup>1-6</sup> but also can be fabricated with solution process using cheap materials.<sup>7-12</sup> The first perovskite solar cell was demonstrated by Miyasaka<sup>13</sup> *et al.* who used lead halide perovskite as the light absorber/sensitizer in a mesoscopic dye-sensitized solar cell. Later study show that perovskite materials has bipolar transport properties and therefore can be readily served as the intrinsic absorption layer in an inverted p-i-n device.<sup>14</sup> Compared to the mesoscopic perovskite solar cell which often requires high-temperature (above 450 °C) treatment the inverted perovskite solar cell with an architecture similar to the planner heterojunction organic photovoltaics has the advantage of a low temperature (< 100 °C) solution process, therefore can be adopted in the roll-to-roll production and the flexible devices. In an inverted device layout, perovskite film was deposited on top of the hole transporter which is generally an organic materials such as PEDOT:PSS. It is very difficult to fabricate perovskite film with large crystalline domains (> 1 μm) and full surface coverage on the smooth surface of an organic compound *via* simple (spin-coating) solution process. Nevertheless, the morphology of perovskite is one of the most important factors to the device performance.<sup>15</sup> One of the strategies to fabricate highly crystalline and continuous perovskite film is using an additive.

The concept of additive was widely used in the bulk-heterojunction organic solar cell to manipulate the morphology of the active layer to enhance the photovoltaic performance of the devices.<sup>16-20</sup> The function of the additive is to reduce the aggregation of n-type fullerene and enhance the crystallinity of the self-organized p-type polymer by its selective solubility towards one component to form an optimal

morphology for facile charge separation and carrier transport. The concept of additive has also been used in perovskite solar cell to improve the morphology of perovskite film to increase the device efficiency. Im<sup>21</sup> *et al.* had added H<sub>2</sub>O or HBr<sub>(aq)</sub> in CH<sub>3</sub>NH<sub>3</sub>PbBr<sub>3</sub>/DMF precursor solution to grow highly dense perovskite film on mesoporous TiO<sub>2</sub> film. Jen<sup>22,23</sup> *et al.* used 1,8-diiodooctane (DIO) as an additive in the precursor solution to reduce the crystallization rate of perovskite upon spin coating. They believed that the bidentate halogenated additives can temporarily chelate with Pb<sup>+2</sup> to increase the solubility of perovskite during the crystal growth to form smooth and continuous film on the flat surface. NH<sub>4</sub>Cl,<sup>24</sup>  $\gamma$ -butyrolactone (GBL),<sup>25</sup> 1-chloronaphthalene (CN)<sup>26</sup> and aminovaleric acid<sup>27</sup> have been used as the additive in CH<sub>3</sub>NH<sub>3</sub>PbI<sub>3</sub> precursor solution to improve the quality of the spin coated film by reducing the crystallization rate of perovskite.

Not only adding additive but also the film post treatment can increase the quality of perovskite film. Recently Yang<sup>28</sup> *et al.* showed that moisture can assist the grain growth of perovskite film to dramatically increase the carrier mobility and charge carrier lifetime. Moisture was known to be an important factor in perovskite solar cell technology with advantages<sup>5,28-29</sup> as well as disadvantages.<sup>30</sup> It seems that water can decompose the structure of ionic perovskite into PbI<sub>2</sub> and MAI, but it can also mend the interface (by dissolution and recrystallization) of the grains to form continuous smooth film. Combining the concept of additive and the function of water, instead of manipulating the nucleation and growth of perovskite film by varying the compositions of the precursor solution in one-step method,<sup>12,15,31-32</sup> we will apply water as an additive on the two-step method<sup>34,35</sup> we used for preparing perovskite film. Our novel approach is to make high quality and full coverage PbI<sub>2</sub> film on PEDOT:PSS by adding controllable amount of water in PbI<sub>2</sub>/DMF to make a concentrated, homogeneous precursor solution. After adding MAI, extremely smooth,

highly crystalline, adhesive and continuous perovskite film was made. The resulting inverted solar cell achieves the highest efficiency of *ca.* 18% with a remarkably high fill factor of 85% which is the highest value amongst all perovskite solar cells.

The preparation steps for perovskite film are the same as what we reported previously<sup>10</sup>: PbI<sub>2</sub> film was spin-coated on PEDOT:PSS deposited ITO and then MAI was added to form perovskite. The detailed device fabrication procedures were described in the experimental section. PEDOT:PSS is an excellent hole transporting material. Nevertheless, to form a crystal homogeneous over a smooth organic surface such as PEDOT:PSS film *via* simple solution process (such as spin-coating) is not easy for an ionic material (such as perovskite) which crystallizes very fast.<sup>12,36-38</sup> On the other hand, compared to perovskite, PbI<sub>2</sub> is less polar therefore can form a continuous film on PEDOT:PSS surface easier. That is the reason that two-step spin coating method is a proper way to fabricate perovskite film when PEDOT:PSS was used as a hole transport layer in the inverted device. DMF (dimethylformamide) is a general solvent for PbI<sub>2</sub>, we found that PbI<sub>2</sub> has low solubility in dried DMF, and a colloid suspension instead of homogeneous solution was formed when 0.74 g of PbI<sub>2</sub> was dissolved in 1 mL DMF (0.80 M, a concentration to obtain PbI<sub>2</sub> film with proper thickness by spin coating) and heat at 80 °C for 10 min. Surprisingly, when a small amount (0.5 ~ 4 vol% *vs* DMF) of H<sub>2</sub>O was added in PbI<sub>2</sub>/DMF, the solutions turn to homogeneous as the photos displayed in Figure 1. H<sub>2</sub>O is miscible with DMF, the polarity, dielectric constant and solubility parameter<sup>39</sup> of DMF changed when H<sub>2</sub>O was added. PbI<sub>2</sub> is also dissolved sparingly in H<sub>2</sub>O and the solubility parameter of DMF/H<sub>2</sub>O mixture may be close to that of PbI<sub>2</sub>, therefore PbI<sub>2</sub> was totally dissolved in the mixed solvent.

The SEM images of PbI<sub>2</sub> films (PbI<sub>2</sub>-X, represented the films prepared from PbI<sub>2</sub>/DMF solution with X vol% (*vs* DMF)) of water deposited on PEDOT:PSS by

spin coating were illustrated in Figure 2. It was shown that the content of H<sub>2</sub>O in the precursor solution has a large impact on the morphology of PbI<sub>2</sub> films. Full coverage, continuous PbI<sub>2</sub> films (PbI<sub>2</sub>-2 and PbI<sub>2</sub>-3) were obtained only when the precursor solution contains 2 ~ 3 wt% H<sub>2</sub>O. More or less water content in the precursor solution results in poorer morphology. Non-continuous film with large voids and rough surface was observed when the precursor solution contains no H<sub>2</sub>O. PbI<sub>2</sub>-2 film prepared from PbI<sub>2</sub>/DMF containing 2 wt% water is the smoothest film composed of the largest grains. High quality PbI<sub>2</sub> films were formed because of the precursor solutions are very homogeneous. Moreover, PEDOT:PSS is hydrophilic; PbI<sub>2</sub>/DMF+H<sub>2</sub>O solution has good adhesion on PEDOT:PSS film. The precursor solution can disperse evenly on the surface of PEDOT:PSS film, improve the surface coverage of PbI<sub>2</sub> film after spinning by matching the interfacial energy.

The crystallinity of PbI<sub>2</sub> films prepared with the precursor solutions containing various amount of water are not the same. GIWXR patterns (from the line scans along the  $q_z$  ( $2\theta$ ) direction) of PbI<sub>2</sub> films are displayed in Figure 3 and the original data were placed in Figure S1 of the Electronic Supporting Information, ESI. The diffraction peaks at  $2\theta$  of 12.3, 25.6 and 38.2 degree indicated clearly that all PbI<sub>2</sub> films are crystalline with the same d-spacing. The crystallinity of PbI<sub>2</sub> film increases when H<sub>2</sub>O was added in the precursor solution but water molecules did not insert into the layer spacing of PbI<sub>2</sub> lattice. The crystallinity and crystalline domain of the films (estimated from the intensity and peak-width of the (001) diffraction peak and listed in Table S1, ESI) are also correlated with the film morphology: smoother film has higher crystallinity and larger crystalline domains. Nevertheless, except PbI<sub>2</sub>-0 film, the variation in crystallinity and crystalline domain size is not significant. Interestingly, the Pole Figures (displayed in the inset of Figure 3) of (001) diffraction peak constructed from the 2D diffraction patterns clearly reveal that PbI<sub>2</sub> film on

PEDOT:PSS has a preferred orientation with its (001) crystal plane parallel to the substrate due to  $\text{PbI}_2$  has hexagonal layered structure. The strong and narrow peak width (*ca.* 20 degree) along the  $\chi$  axis confirmed that  $\text{PbI}_2$ -2 and  $\text{PbI}_2$ -3 films are highly oriented on PEDOT:PSS surface even the film was prepared with spin coating at room temperature. The increased coverage and smoothness of  $\text{PbI}_2$  film assisted with  $\text{H}_2\text{O}$  additive suggests that water can induce the homogenous nucleation by modifying the  $\text{PbI}_2$ /PEDOT:PSS interfacial energy. Therefore  $\text{PbI}_2$  crystal can grow evenly and has the best contact with PEDOT:PSS surface.

$\text{CH}_3\text{NH}_3\text{PbI}_3$  films were fabricated by spin coating of MAI/isopropanol (IPA) solutions with various concentrations at a fixed spin program of 2000 rpm for 30 seconds. The best performance perovskite film was obtained when 30  $\mu\text{L}$ , 5% MAI/IPA was used for reacting with  $\text{PbI}_2$  films. In the two-step spin coating method, the quality of perovskite film may depend on the morphology and crystallinity of the starting  $\text{PbI}_2$  film. SEM surface images of perovskite films (Prov-X, Prov-X means the film prepared from  $\text{PbI}_2$ -X film) were displayed in Figure 4. As expected the morphology of perovskite films was affected significantly by their starting  $\text{PbI}_2$  films. Films (Prov-2 ~ Prov-3) prepared from good quality  $\text{PbI}_2$  films ( $\text{PbI}_2$ -2 and  $\text{PbI}_2$ -3) is very smooth and densely packed. There is almost no hole or crevice between the grains. This is the advantage for preparing perovskite film using two-step (spin-coating) method because of making a high quality  $\text{PbI}_2$  film is easier than fabricating a good perovskite film. The morphology of perovskite film is a determining parameter on the photovoltaic performance of the corresponding solar cell, which will be discussed more in the later paragraphs.

The GIXRD patterns of perovskite films illustrated in Figure 5 have seven characteristic peaks at  $2\theta$  from 10 to 35 degree, confirmed that only tetragonal perovskite structure<sup>13,40,41</sup> was formed for all films. This is another advantage for

fabricating perovskite film using two-step method since highly pure perovskite can be obtained by controlling the volume and concentration of MAI/IPA solution. Surprisingly, the variation in the crystallinity for perovskite films is different from their ancestor  $\text{PbI}_2$  films. The crystallinity (peak intensity) of all perovskite films is similar and only Prov-0 and Prov-4 have slightly lower crystallinity than the others. Nevertheless, Prov-2 and Pero-0 films have the largest and smallest crystalline domain size, respectively, consistent with the surface morphology displayed in Figure 4.

After spin coating a PCBM film, solvent annealed of PCBM acceptor layer and employing Ca/Al electrode using thermal evaporation, the inverted perovskite cell with ITO/PEDOT:PSS/perovskite/PCBM/Ca/Al architecture<sup>42</sup> was fabricated. The photovoltaic parameters of the highest efficiency cells of D-X (D-X means the solar cell based on Prov-X film) were summarized in Table 1 and the corresponding I-V curves were displayed in Figure S2, ESI. We fabricated 20 cells in each preparation condition (listed in Table 1) and the efficiency statistical analysis was illustrated in Figure S3, ESI. Data in Table 1 reveal that the efficiency of perovskite solar cell depends on the quality of the starting  $\text{PbI}_2$  film which is very sensitive to the water content in its precursor solution. The photovoltaic performance of the device based on Prov-0 film (film prepared without water additive) is very poor. Small amount (0.5 wt%) of water additive in  $\text{PbI}_2$  precursor solution can improve significantly all the photovoltaic parameters of the resulting cells and the overall efficiency increases from 0.0063% to 7.4%. Cell exhibited the highest efficiency of 18% with remarkable FF of 0.85 was obtained when Prov-2 film was applied as a light absorber. Further increases the amount of water additive in  $\text{PbI}_2$  precursor solution, the efficiency of the corresponding cell decreases again. We reported previously<sup>20</sup> that the device with efficiency up to 16% was obtained based on similar cell fabrication procedures

without knowing the exactly water content in  $\text{PbI}_2/\text{DMF}$  precursor solution. The results disclose that to obtain high efficiency and reproducible perovskite solar cell, the materials, fabrication steps and environment should be precisely controlled. At the same time it also indicated that perovskite cell with higher efficiency can be expected in the future as more properties of the components in the cell were known.

The IPCE and I-V curves for the champion cell (D-2 with  $\eta$  of 18%) are displayed in Figure 6. The IPCE curve shows a strong spectral response in the range from 350 nm to 750 nm with efficiency close to 90% at the wavelength of 566 nm. The integrated current ( $19.8 \text{ mA cm}^{-2}$ ) from the IPCE curve is *ca.* 4% mismatch compared to the  $J_{sc}$  ( $20.6 \text{ mA cm}^{-2}$ ) obtained from the I-V curve. A slightly mismatch of the  $J_{sc}$  from the I-V curves and calculated from IPCE data is a general phenomenon in solar cells since the measuring bases are not totally the same and there exist a measuring uncertainty of the current density. It is notable that the champion cell has extremely high  $FF$  of 0.85, the highest value amongst all perovskite solar cell reported in literature.<sup>43</sup> We believe that high quality (especially good morphology) of the absorber is the key parameter for achieving such high  $FF$  for the inverted perovskite solar cells. It was known that the series resistance ( $R_s$ ) of the device expresses the integral conductivity of the device directly related to its internal carrier mobility whereas the shunt resistance ( $R_{SH}$ ) refers to the loss of photocurrent through carrier recombination within the device, particularly at the interfaces of each layer. Shunt resistance is typically due to the manufacturing defects, rather than poor solar cell design.  $R_s$  and  $R_{SH}$  calculated from the I-V curves of the corresponding devices were also listed in Table 1. The champion cell (D-2) reported in this article has a series resistance as low as  $1.54 \text{ } \Omega \cdot \text{cm}^2$  and extremely high  $R_{SH}$  of  $87 \times 10^3 \text{ } \Omega \cdot \text{cm}^2$ . Small  $R_s$  suggests that the interphase contact is good and the conductivity of every layers of the device is high. High shunt resistance indicates that the power loss in

solar cell through an alternate current path is very small, resulting in high  $FF$ . In order to check the reproducibility of the high  $FF$ , 50 devices (during one month) were fabricated and the  $FF$  was recorded. The histogram of the  $FF$  based on 50 devices (displayed in Figure S4, ESI) reveals that the high  $FF$  is a general result for the inverted devices based on perovskite film prepared from  $PbI_2$  film with 2 wt%  $H_2O$  in its precursor solution.

To get more in-depth understanding the origin of the high  $FF$  of the champion cell, the information of the layer stacking was investigated. The SEM cross section images of ITO/PEDOT:PSS/Prov-2 film was shown in Figure 7 (the image of Prov-0 film is also displayed in Figure 7 for comparison). The preparation condition of these perovskite films was identical to the conditions used for the device fabrication. Prov-0 (obtained from the  $PbI_2$  film prepared without  $H_2O$  additive) composed of large numbers of small crystallites (size 50 nm ~ 500 nm) with lots of voids. On the other hand, Prov-2 is a very dense film with large grains. No pinhole was observed even at the magnification of 100,000. The thickness of the films estimated from the cross-section images for Prov-1 and Prov-4 is 550 and 410 nm, respectively. Prov-4 film has similar absorption intensity (unpublished result) but thinner compared to Prov-1 film consistent with the SEM images which reveal that Prov-2 is a denser film. The grain size of Prov-2 estimated from the cross section image is 0.5 ~ 1.0  $\mu m$  in width, which is close to that calculated from the surface morphology. Notably the length of the grains is equal to the thickness of the film and the film uniformity extends to several tens micrometer as the image displayed in Figure 7(c). The structure of the film cross-section provides a good reason to explain why the cell using rather thick (410 nm) perovskite film can achieve so high  $FF$ . It seems that the morphology rather than the crystallinity of perovskite film is a key parameter for the photovoltaic performance of the corresponding inverted perovskite solar cells,

consistent with the conclusion made by Snaith<sup>12</sup> *et al.* Furthermore, Xiao<sup>44</sup> *et al.* also used two-step method to prepare perovskite film and heat the film to trigger the inter-diffusion between  $\text{PbI}_2$  and MAI. The resulting inverted cell exhibited an efficiency of 15.4% and the maximum grain size of perovskite film was around 260 nm.<sup>45</sup> The efficiency of the cell and the grain size of perovskite absorber reported by Xiao<sup>44</sup> *et al.* are lower than those of our device. It is probably due the water content in  $\text{PbI}_2$  precursor solution is not well controlled (DMF may absorb water from the ambient atmosphere if it is not well-maintained) in Xiao's paper.<sup>44</sup> Therefore, poorer quality  $\text{PbI}_2$  film was formed in the first step although the paper did not discuss the morphology of  $\text{PbI}_2$  film. Xiao<sup>45</sup> *et al.* later used solvent (DMF) annealing to improve the quality of perovskite film prepared by inter-diffusion method. The surface morphology and crystallite size of the solvent annealed perovskite film is improved nevertheless the cross-section image revealed that the film was composed of large number of crystallites with the size smaller than the thickness of film. High inter-particle contact resistance exists in the film therefore the efficiency of their best device is only 15.6% with a FF of *ca* 80%. The higher Voc and FF of the device reported in this paper is due to the perovskite film we fabricated has better quality compared to what we reported<sup>20</sup> before and most perovskite films reported in literature.<sup>14,44,45</sup>

It was known that perovskite solar cells may show photocurrent hysteresis at certain voltage scanning rates (or sweep delay times) or scan directions. The photocurrent hysteresis may be due to either the charge traps of the low quality perovskite film, unbalanced electron and hole transport rate or the defect in the interphase.<sup>46,47</sup> Therefore the efficiency reported for a device with photocurrent hysteresis may not truly represent the performance of the device. We found that high efficiency cell with inverted architecture generally shows no current hysteresis. The

*I-V* curves (displayed in Figure S5, ESI) of D-2 (D-X device means the device based on Prov-X film) cell scanned at two different directions and scan rates (0.01~ 0.5 V/sec) show no hysteresis. The results also suggested that the hysteresis in photocurrent is more likely due to the defects on perovskite film and the interfaces of PEDOT:PSS/perovskite/PCBM, which can be eliminated partly by using high quality perovskite film prepared with the novel approach. Two-step spin-coating is a preeminent method to prepare highly crystalline and continuous perovskite film. In the two-step method, the quality of MAPbI<sub>3</sub> film depends on the film quality of PbI<sub>2</sub>. To prepare highly dense and smooth PbI<sub>2</sub> film on the surface of PEDOT:PSS is easier compared to deposit perovskite film because of PbI<sub>2</sub> is less ionic than MAPbI<sub>3</sub>. High quality PbI<sub>2</sub> film can be prepared by simply adding small amount of water in the precursor solution.

In the development of perovskite solar cells, high efficiency device sometimes shows poor long-term stability.<sup>5</sup> The high efficiency device reported in this paper shows very good long term stability when stored in the glove box as illustrated in Figure 8. The PCE of the device decreases less than 10% after 40 days stored under dark in a glove box. Furthermore we also test the stability of the device under illuminating with AM 1.5 G (100 mW/cm<sup>2</sup>) light. The efficiency decreases *ca.* 4% gradually in the first 4 hours and then stabilizes up to 6 hours (the test time, see Figure S6, ESI). Another issue generally concerned by perovskite solar cell community is the reproducibility of the photovoltaic performance for the cells fabricated at almost the same condition, due to the fast crystallization of perovskite absorber is difficult to control. The statistical data of the efficiency based on 20 cells fabricated for each condition (listed in Table 1) shown in Figure S3, ESI revealed that the inverted perovskite cells fabricated with the method reported in this paper are quite reproducible. More detail analysis was done for the 20 devices (D-2) fabricated with 2

wt% H<sub>2</sub>O in PbI<sub>2</sub>/DMF precursor solution (the condition for fabricating cell with the highest efficiency). The histograms and detail statistical analysis using quartile deviation method<sup>48</sup> of the photovoltaic parameters of D-2 cells were illustrated in Figure S7 and Table S2 (ESI), respectively. As the statistical point of view, none of the data displayed in Table S2 is an outlier (outlier means non-reasonable datum). In other words, the photovoltaic data of the 20 devices suggested that the devices are reproducible using the fabrication method reported in this paper.

The efficiency measurement containing uncertainty which should be analyzed in order to show the confidence of the data reported. The uncertainty (error) of a measurement comes from the random errors and systematic errors. The random errors of the photovoltaic parameters were illustrated in Table S3, ESI and the detailed procedures for determining random errors can be found in the experimental section. The most significant systematic errors (they are very time-consuming to determine since they involve so many parameters compared to the general chemical analysis) of the efficiency measuring systems and the resulting photovoltaic parameters are listed in Table S4 and Table S5, ESI. If the standard uncertainty (with the coverage factor ( $k$ ) = 1) or expanded uncertainty (with the coverage factor ( $k$ ) = 2) was concerned, the data listed in Table S2 are all within the experimental uncertainty.

In conclusion, we report a strategy to synthesize high quality perovskite film under ambient atmosphere at low temperature using a two-step method. A few percent of most environmental friendly chemical (H<sub>2</sub>O) was added into PbI<sub>2</sub>/DMF to make a homogeneous solution. PbI<sub>2</sub> film spin coated on PEDOT:PSS coated ITO (from the homogeneous precursor solution) is highly smooth, crystalline and oriented with its (001) plane parallel to the surface of the substrate. Perovskite film fabricated from the high quality PbI<sub>2</sub> film is highly pure and dense even without any pinhole. The champion inverted cell based on high quality perovskite film achieves the power

conversion efficiency of *ca.* 18% with a remarkable high FF of 0.85 which is the highest value amongst perovskite solar cells. The FF value is also very reproducible: less than 10% deviation for 50 cells. The cell exhibits no current hysteresis and stable under dark and illumination in dry and inert atmosphere. The results provide a new way to fabricate highly crystalline and full coverage dense perovskite film on very smooth PEDOT:PSS surface. This article also reveals that how water additive in  $\text{PbI}_2/\text{DMF}$  precursor solution can affect the surface coverage of  $\text{PbI}_2$  and perovskite film (prepared with two-step method) on PEDOT:PSS and the photovoltaic performance of the corresponding inverted solar cell.

## Experimental

**Materials and Physicochemical Studies.** Aqueous dispersion of PEDOT:PSS (1.3~1.7 wt%, from H.C. Stark Baytron P AI 4083) was obtained from Heraeus Co.  $\text{PC}_{71}\text{BM}$  (99.5%) was purchased from Solenne B. V., Netherlands.  $\text{PbI}_2$  (99.999%) was purchased from Aldrich Co. All the above materials were used as received. ITO-covered glass substrates purchased from Merck Co. were photolithographically patterned in our laboratory with  $\text{HCl}_{(\text{aq})}$ .  $\text{CH}_3\text{NH}_3\text{I}$  (MAI) was synthesized with the same method published in literature.<sup>49</sup> The thickness of the films was measured with a depth-profile meter (Veeco Dektak 150, USA). Five lines on the 1.0 cm x 1.0 cm film were made by carefully scratching with a tip and the average height between the hills and valleys is used to represent the film thickness. GIXRD data were collected in the  $2\theta$  range 5 ~ 50 degree on a Bruker powder diffractometer (D8 Discover) using  $\text{Cu K}\alpha 1$  radiation equipped with a 2D detector. Scanning Electron Micrograph (SEM) was performed with a Hitachi S-800 microscopy at 15 KV. Samples (surface and cross-section of the film on substrates) for SEM imaging were mounted on a metal stub with a piece of conducting tape then coated with a thin layer of gold film to avoid

charging.

**Device Fabrication.** PEDOT:PSS was spin-coated on a heat pretreated patterned ITO under 5000 rpm for 50 sec and then annealed at 100 °C for 15 min.  $\text{PbI}_2$ /DMF precursor solutions with  $\text{H}_2\text{O}$  additive were prepared by first dissolving  $\text{PbI}_2$  in DMF, then adding various amount of  $\text{H}_2\text{O}$  in the solution and stirring overnight. For depositing perovskite layer, first a layer of  $\text{PbI}_2$  was spin-coated on top of PEDOT:PSS coated ITO substrate from 0.8 M precursor solution (with or without  $\text{H}_2\text{O}$  additive). Before  $\text{PbI}_2$  was dried totally,  $\text{CH}_3\text{NH}_3\text{I}$  was spin-coated on top of  $\text{PbI}_2$  film from isopropanol solution with various concentrations at spin rates of 2000 rpm to form perovskite film. Specifically, the best photovoltaic performance perovskite film was fabricated by using 30  $\mu\text{L}$ , 50 mg/mL  $\text{CH}_3\text{NH}_3\text{I}$ /IPA solution at the spin rate and time of 2000 rpm and 30 sec. Acceptor layer was prepared by spin coating (1000 rpm, 30 sec) 2 wt%  $\text{PC}_{71}\text{BM}$  in chlorobenzene onto the surface of perovskite film. The  $\text{PC}_{71}\text{BM}$  film was solvent annealed by covering the film with a petri dish for 24 hour. The trace amount of solvent (chlorobenzene) in the film will continuously infiltrate  $\text{PC}_{71}\text{BM}$  to form a close contact with the perovskite film underneath. Solvent annealing of the  $\text{PC}_{71}\text{BM}$  layer is very important when the surface of perovskite film is rather rough. However it has less effect when the quality (flat and continuous) of perovskite film is good as the high-efficiency cell reported in this study. All the fabrication procedures were carried in the ambient atmosphere at low temperature ( $\leq 100$  °C). Finally, the PEDOT:PSS/perovskite/ $\text{PC}_{71}\text{BM}$  film was transferred to a vacuum chamber for coating Ca/Al (20 nm/100 nm) electrode.

**Photovoltaic performance Measurement.** The Sun simulator used in this study is 3A

(AAA) Wacom solar simulator (KXL-500F, Wacom, Japan). The light intensity of the simulator was calibrated with a KG-5 Si diode before each measurement. The Si diode was calibrated from time to time with a Secondary-Reference Si-cell (For example, the current of the Secondary-Reference single crystal Si-cell with KG-2 filter (2.0 cm x 2.0 cm in size) under 1 Sun should be 70.6 mA) which was calibrated by TERTEC Org., Taiwan (following the IEC 60904). The area of the test cell was defined by a home-made mask. The area (was defined with the close polyline to a polygon) of the mask was measured with a microscope (PS-930 NG, Just Technology Corp., Taiwan) having the accuracy of 0.001 cm. 10 times repeatedly measurements were performed to get the average value of the mask area. A Keithley 4200 source measuring unit was used to apply voltage and measure current. The efficiency of the cell was calculated by  $(P_{\max})/(L \times A)$  ( $P_{\max}$  is the maximum power of the I-V curve and L is the intensity of the simulated light, A is the area of mask on the test cell). FF was calculated by  $(P_{\max})/(J_{sc} \times V_{oc})$ .  $J_{sc}$  is equal to  $I_{sc}$  divided by the area of test cell (defined by the mask).

IPCE of the perovskite solar cell was measured using an IPCE measuring system (QE-R3011, Enlitech Inc., Taiwan). QE-R3011 equipped with a Xe lamp as the light source and the spectral resolution of the mono-chromator is 1 nm. The wavelength interval we used for measuring the IPCE curve is 10 nm. The intensity of the incident light from the mono-chromator was calibrated with a Si-reference cell installed inside QE-R3011. The calibration of the light intensity was done before each IPCE measurement. The beam size of the incident light is smaller than the area of the device (without mask) for the correct measurements. The Si-reference cell was calibrated from time to time with a Secondary-Reference Si-cell (the same as that used to calibrate the Sun simulator). The temperature of the lab for the Photovoltaic performance measurements is  $25 \pm 5$  °C but the temperature of the test cell is stable

up to  $\pm 2$  °C under the illumination of the light within 30 minutes.

For understanding the uncertainty of the efficiency for the high performance inverted perovskite solar cells, the random and systematic errors (uncertainties) were also analyzed. The uncertainty of a measurement comes from the random errors and systematic errors. To present a random error for the photovoltaic performance measurements, the photovoltaic parameters of a stable reference diode were repeatedly measured 10 times. It is very time-consuming to get the systematic error of the photovoltaic parameters since it involves so many parameters. However the uncertainty data should be measured after the measuring system is set and calibrated the measuring system from time to time. The systematic error involved Instrument errors, Method errors and Personal errors which were determined by many sophisticated procedures. Some most important (big) errors were displayed in Table 4 and the origins of the errors were explained below the table. Finally the errors (expressed as standard uncertainty with the coverage factor ( $k$ ) = 1 and expanded uncertainty with the coverage factor ( $k$ ) = 2) of the photovoltaic parameters propagated from the corresponding items of the measuring errors were calculated.

### Acknowledgements

Financial support from the Ministry of Science and Technology (MOST), Taiwan, ROC (grand number: NSC101-2113-M-008-008-MY3) is gratefully acknowledged. MG thanks financial support from SNF-NanoTera (SYNERGY) and Swiss Federal Office of Energy (SYNERGY). The devices fabrication was carried out in Advanced Laboratory of Accommodation and Research for Organic Photovoltaics, MOST, Taiwan, ROC.

**Supporting Information Available:**

Supplementary data are collected in the Electronic Supporting Information (ESI).

This material is available online with the article.

## References:

- 1 R. F. Service, *Science*, 2014, **344**, 458-458.
- 2 N-G. Park, *J. Phys. Chem. Lett.*, 2013, **4**, 2423–2429.
- 3 M. D. McGehee, *Nature*, 2013, **501**, 323-325.
- 4 National Renewable Energy Laboratory, Best Research Cell Efficiency. ([http://www.nrel.gov/ncpv/images/efficiency\\_chart.jpg](http://www.nrel.gov/ncpv/images/efficiency_chart.jpg))
- 5 H. Zhou, Q. Chen, G. Li, S. Luo, T. Song, S.-H. Duan, Z. Hong, J. You, Y. Liu, Y. Yang, *Science*, 2014, **345**, 542-546.
- 6 M. M. Lee, J. Teuscher, T. Miyasaka, T. N. Murakami, H. J. Snaith, *Science*, 2012, **338**, 643-647.
- 7 H. J. Snaith, *J. Phys. Chem. Lett.*, 2013, **4**, 3623-3630.
- 8 S. Kazim, M. K. Nazeeruddin, M. Grätzel, S. Ahmad, *Angew. Chem. Int. Ed.*, 2014, **53**, 2812-2824.
- 9 J. You, Z. Hong, Y. Yang, Q. Chen, M. Cai, T.-B. Song, C.-C. Chen, S. Lu, Y. Liu, H. Zhou, Y. Yang, *ACS Nano*, 2014, **8**, 1674-1680.
- 10 C.-H. Chiang, Z.-L. Tseng, C.-G. Wu, *J. Mater. Chem. A*, 2014, **2**, 15897-15903.
- 11 S. Sun, T. Salim, N. Mathews, M. Duchamp, C. Boothroy, G. Xing, T. C. Sumbc, Y. M. Lam, *Energy Environ. Sci.*, 2014, **7**, 399-407.
- 12 G. E. Eperon, V. M. Burlakov, P. Docampo, A. Goriely, H. J. Snaith, *Adv. Funct. Mater.*, 2014, **24**, 151-157.
- 13 A. Kojima, K. Teshima, Y. Shirai, T. Miyasaka *J. Am. Chem. Soc.*, 2009, **131**, 6050-6051.
- 14 M. Liu, M. B. Johnston, H. J. Snaith, *Nature*, 2013, **501**, 395-398.
- 15 P. Docampo, J. M. Ball, M. Darwich, G. E. Eperon, H. J. Sniath, *Nat. Commun.*, 2013, **4**, 2761-2766.
- 16 H.-Y. Chen, H. Yang, G. Yang, S. Sista, R. Zadoyan, G. Li, Y. Yang, *J. Phys. Chem.*

- C, 2009, **113**, 7946-7963.
- 17 P. Jeffrey, L. S. Michelle, J. H. Alan, C. B. Guillermo, *Adv. Mater.*, 2009, **21**, 1521-1529.
- 18 M.-S. Su, C.-Y. Kuo, M.-C. Yuan, U.-S. Jeng, C.-J. Su, K.-H. Wei, *Adv. Mater.*, 2011, **23**, 3315-3319.
- 19 J. S. Moon, C. J. Takacs, S. Cho, R. C. Coffin, H. Kim, G. C. Bazan, A. J. Heeger, *Nano Lett.*, 2010, **10**, 4005-4008.
- 20 C.-G. Wu, C.-H. Chiang, H.-C. Han, *J. Mater. Chem. A*, 2014, **3**, 5295-5303.
- 21 J. H. Heo, D. H. Song, S. H. Im, *Adv. Mater.*, 2014, **26**, 8179-8183.
- 22 P.-W. Liang, C.-Y. Liao, C.-C. Chueh, F. Zuo, S. T. Williams, X.-K. Xin, J. Lin, A. K.-Y. Jen, *Adv. Mater.*, 2014, **26**, 3748-3754.
- 23 C.-C. Chueh, C.-Y. Liao, F. Zuo, S. T. Williams, P.-W. Liang, A. K.-Y. Jen, *J. Mater. Chem. A*, DOI: 10.1039/c4ta05012f.
- 24 C. Zuo, L. Ding, *Nanoscale*, 2014, **6**, 9935-9938.
- 25 H.-B. Kim, H. Choi, J. Jeong, S. Kim, B. Walker, S. Song, J. Y. Kim, *Nanoscale*, 2014, **6**, 6679-6683.
- 26 X. Song, W. Wang, P. Sun, W. Ma, Z.-K. Chen, *Appl. Phys. Lett.*, 2015, **106**, 033901.
- 27 M. X. Li, L. Liu, Z. Ku, T. Liu, Y. Rong, M. Xu, M. Hu, J. Chen, Y. Yang, M. Grätzel, H. Han, *Science*, 2014, **345**, 295-298.
- 28 J. You, Y. (M.) Yang, Z. Hong, T.-B. Song, L. Meng, Y. Liu, C. Jiang, H. Zhou, W.-H. Chang, G. Li, Y. Yang, *Appl. Phys. Lett.*, 2014, **105**, 183902-183906.
- 29 K. K. Bass, R. E. McAnally, S. Zhou, P. I. Djurovich, M. E. Thompson, B. C. Melot, *Chem. Commun.*, 2014, **50**, 15819-15822.
- 30 J. M. Frost, K. T. Butler, F. Brivio, C. H. Hendon, M. v. Schilfgaarde, A. Walsh, *Nano Lett.* 2014, **14**, 2584-2590.

- 31 J. Y. Jeng, Y. F. Chiang, M. H. Lee, S. R. Peng, T. F. Guo, P. Chen, T. C. Wen, *Adv. Mater.*, 2013, **25**, 3727-3732.
- 32 B. Conings, L. Baeten, C. D. Dobbelaere, J. D'Haen, J. Manca, H. G. Boyen, *Adv. Mater.*, 2014, **26**, 2041–2046.
- 33 N. J. Jeon, J. H. Noh, Y. C. Kim, W. S. Yang, S. Ryu, S. I. Seok, *Nature Mater.*, 2014, **13**, 897–903.
- 34 J. Burschka, N. Pellet, S.-J. Moon, R. Humphry-Baker, P. Gao, M. K. Nazeeruddin, M. Grätzel, *Nature*, 2013, **499**, 316-319.
- 35 D. Bi, S.-J. Moon, L. Häggman, G. Boschloo, L. Yang, E. M. Johansson, Md. K. Nazeeruddin, M. Grätzel, A. Hagfeldt, *RSC Adv.*, 2013, **3**, 18782-18788.
- 36 J. M. Ball, M. M. Lee, A. Hey, H. J. Snaith, *Energy Environ. Sci.*, 2013, **6**, 1739-1743.
- 37 M. J. Carnie, C. Charbonneau, M. L. Davies, J. Troughton, T. M. Watson, K. Wojciechowski, H. J. Snaith, D. A. Worsley, *Chem. Commun.*, 2013, **49**, 7893-7895.
- 38 Q. Wang, Y. C. Shao, Q. F. Dong, Z. Q. Xiao, Y. B. Yuan, J. S. Huang, *Energy Environ. Sci.*, 2014, **7**, 2359-2365.
- 39 A. F. M. Barton, *Handbook of Solubility Parameters and Other Cohesion Parameters, 2nd edition*. CRC Press (1991).
- 40 T. Baikie, Y. Fang, J. M. Kadro, M. Schreyer, F. Wei, S. G. Mhaisalkar, M. Graetzel, T. J. White, *J. Mater. Chem. A*, 2013, **1**, 5628-5631.
- 41 J.-H. Im, C.-R. Lee, J.-W. Lee, S.-W. Park, N.-G. Park, *Nanoscale*, 2011, **3**, 4088-4093.
- 42 O. Malinkiewicz, Y. Aswani, Y. H. Lee, E. Minguez, M. Graetzel, M. K. Nazeeruddin, H. J. Bolink, *Nature Photon.*, 2014, **8**, 128-132.
- 43 D. Liu, T. L. Kelly, *Nat. Photon.*, 2014, **8**, 133-138.

- 44 Z. Xiao, C. Bi, Y. Shao, Q. Dong, Q. Wang, Y. Yuan, C. Wang, Y. Gao, J. Huang, *Energy Environ. Sci.*, 2014, **7**, 2619-2623.
- 45 Z. Xiao, Q. Dong, C. Bi, Y. Shao, Y. Yuan, J. Huang, *Adv. Mater.*, 2014, **26**, 6503-6509.
- 46 H. J. Snaith, *J. Phys. Chem. Lett.*, 2014, **5**, 1511-1515.
- 47 M. R. Filip, G. E. Eperon, H. J. Snaith, F. Giustino, *Nat. Commun.*, 2014, **5**, 5757-5760.
- 48 J.-H. Im1, I.-H. Jang, N. Pellet, M. Grätzel, N.-G. Park, *Nat. Nanotech.*, 2014, **9**, 927-932.
- 49 L. Etgar, P. Gao, Z. Xue, Q. Peng, A. K. Chandiran, B. Liu, M. K. Nazeeruddin, M. Grätzel, *J. Am. Chem. Soc.*, 2012, **134**, 17396-17399.

## Figure captions

Figure 1. The photographs of  $\text{PbI}_2/\text{DMF}$  solutions containing various amount of  $\text{H}_2\text{O}$  additive (the  $\text{H}_2\text{O}$  content is volume ratio *vs* DMF).

Figure 2. SEM images of  $\text{PbI}_2$  films prepared from  $\text{PbI}_2/\text{DMF}$  solutions containing various amount of  $\text{H}_2\text{O}$  additive.

Figure 3. XRD patterns of  $\text{PbI}_2$  films prepared from  $\text{PbI}_2/\text{DMF}$  solutions containing various amount of  $\text{H}_2\text{O}$  additive (insert: the Pole Figure of the pattern (the intensity *vs*  $\chi$  of the 2D diffraction pattern).

Figure 4. SEM images of perovskite films prepared from various  $\text{PbI}_2$  films (Prov-2 means perovskite film prepared from  $\text{PbI}_2$ -2 film).

Figure 5. XRD patterns of various perovskite films (insert: the peak at  $2\theta$  of  $12 \sim 16$  degree).

Figure 6. (a) I-V curve and (b) EQE curve (the integrated current from the EQE curve also displayed) of the champion cell reported in this article.

Figure 7. SEM cross-section images of (a) Prov-0 film (b) Prov-2 film (c) Prov-2 film at lower magnification.

Figure 8. Long-term stability test of the inverted perovskite solar cell (in glove box).

Table 1: The photovoltaic parameters, series resistance ( $R_S$ ) and Shunt resistance ( $R_{SH}$ ) of the inverted cells based on various perovskite films.

<sup>a</sup> Device	<sup>b</sup> H <sub>2</sub> O additive	J <sub>sc</sub> (mAcm <sup>-2</sup> )	V <sub>oc</sub> (V)	FF	<sup>c</sup> η (%)	R <sub>s</sub> (W cm <sup>2</sup> )	R <sub>sh</sub> (Ω cm <sup>2</sup> )
D-0	0 wt%	0.329	0.10	0.19	0.0063	548	3.0x10 <sup>2</sup>
D-0.5	0.5 wt%	13.9	0.89	0.60	7.4	10.1	1.0x10 <sup>3</sup>
D-1	1 wt%	19.1	0.94	0.74	13	4.50	1.1x10 <sup>3</sup>
D-2	2 wt%	20.6	1.03	0.85	18	1.54	8.7 x10 <sup>4</sup>
D-3	3 wt%	19.5	0.98	0.78	15	2.65	1.2 x10 <sup>3</sup>
D-4	4 wt%	14.3	0.92	0.64	8.4	5.90	4.1x10 <sup>2</sup>

a. D-0 means the cell based on Prov-0 film.

b. The H<sub>2</sub>O content is the weight ratio vs DMF.

c. The standard uncertainty and expanded uncertainty (combined the random and systematic errors) in measuring the efficiency are ±4.0% and ±8.0%, respectively (see Table S5 of ESI and the explanations below the table).\_

Figure 1

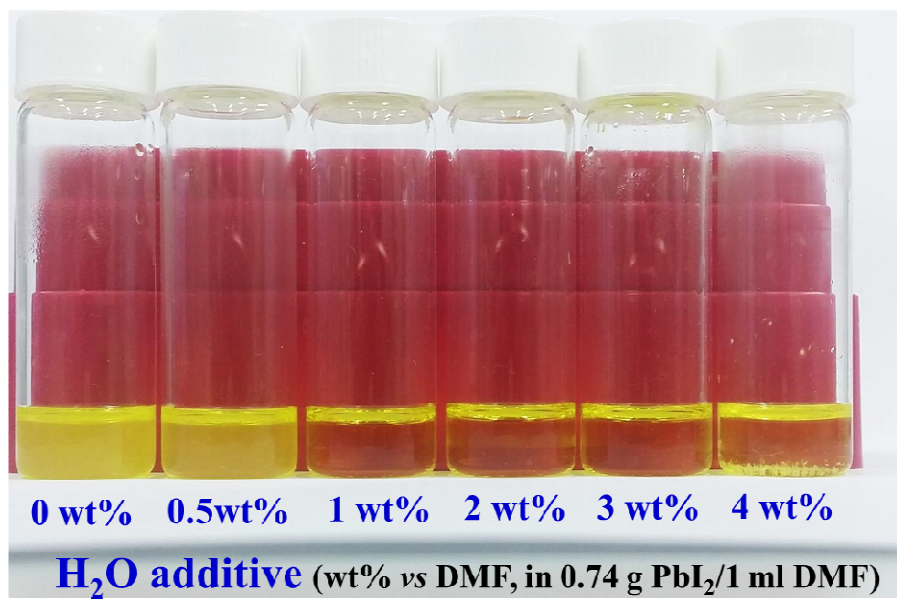


Figure 2

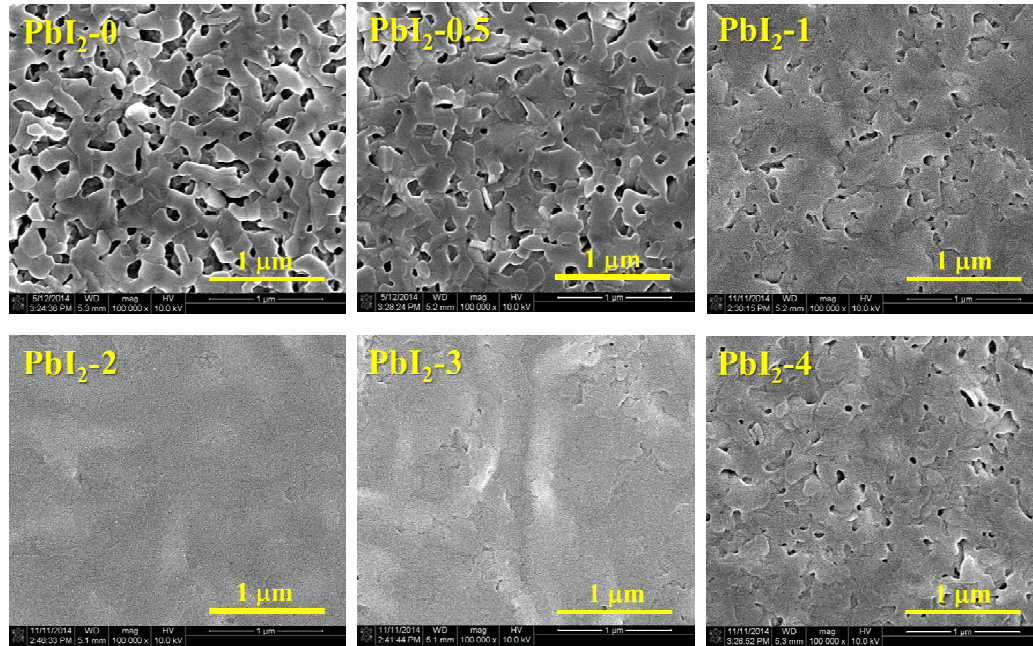


Figure 3

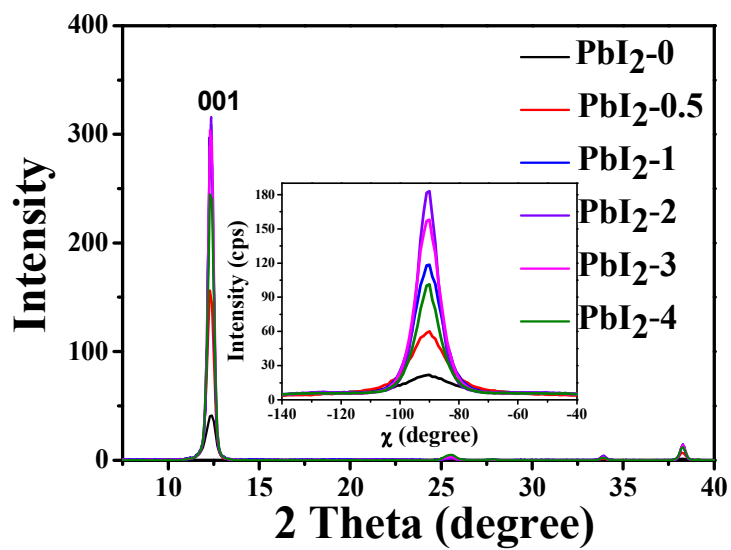


Figure 4

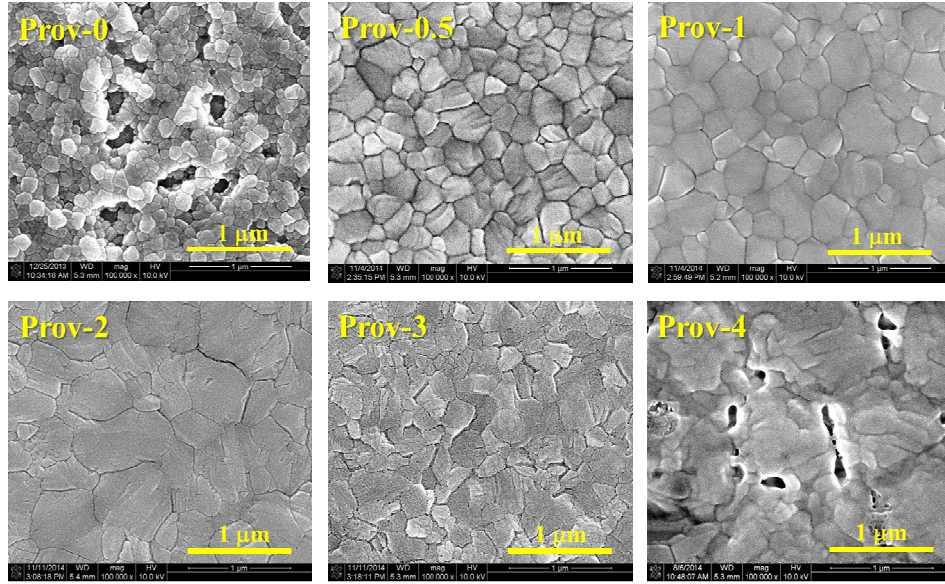


Figure 5

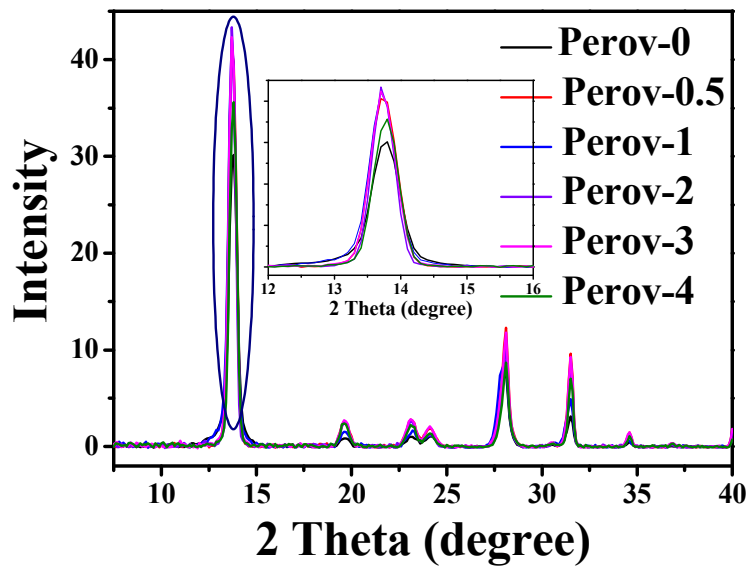


Figure 6

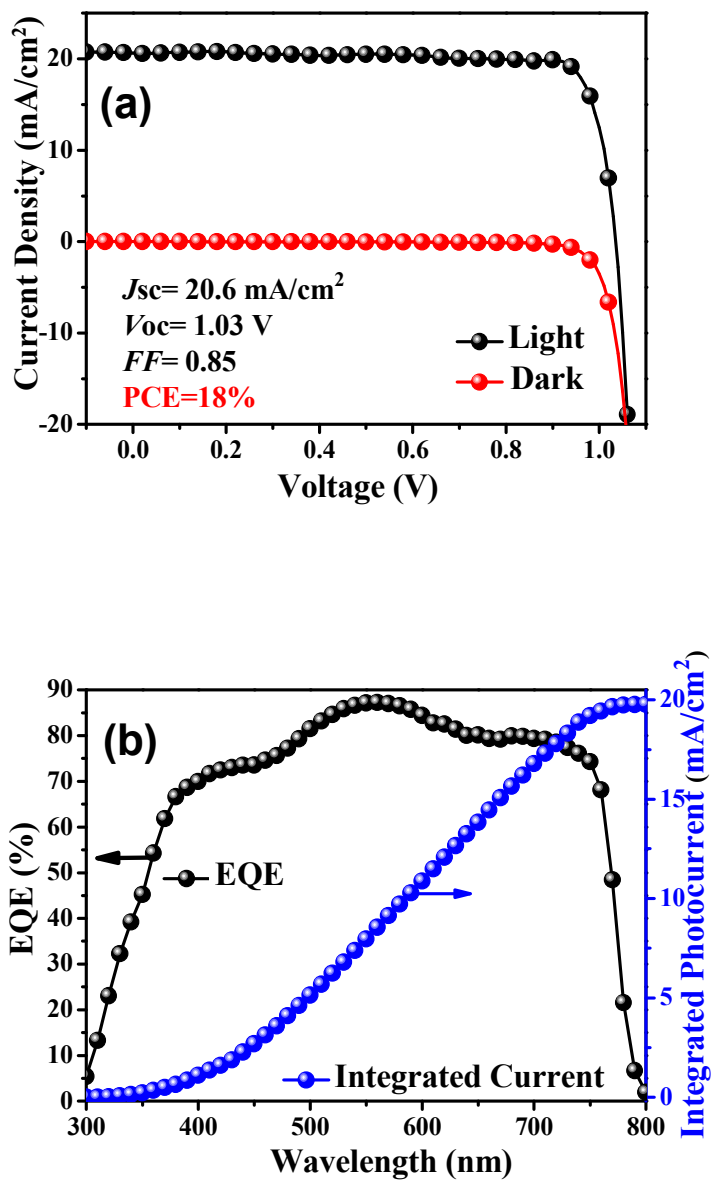


Figure 7

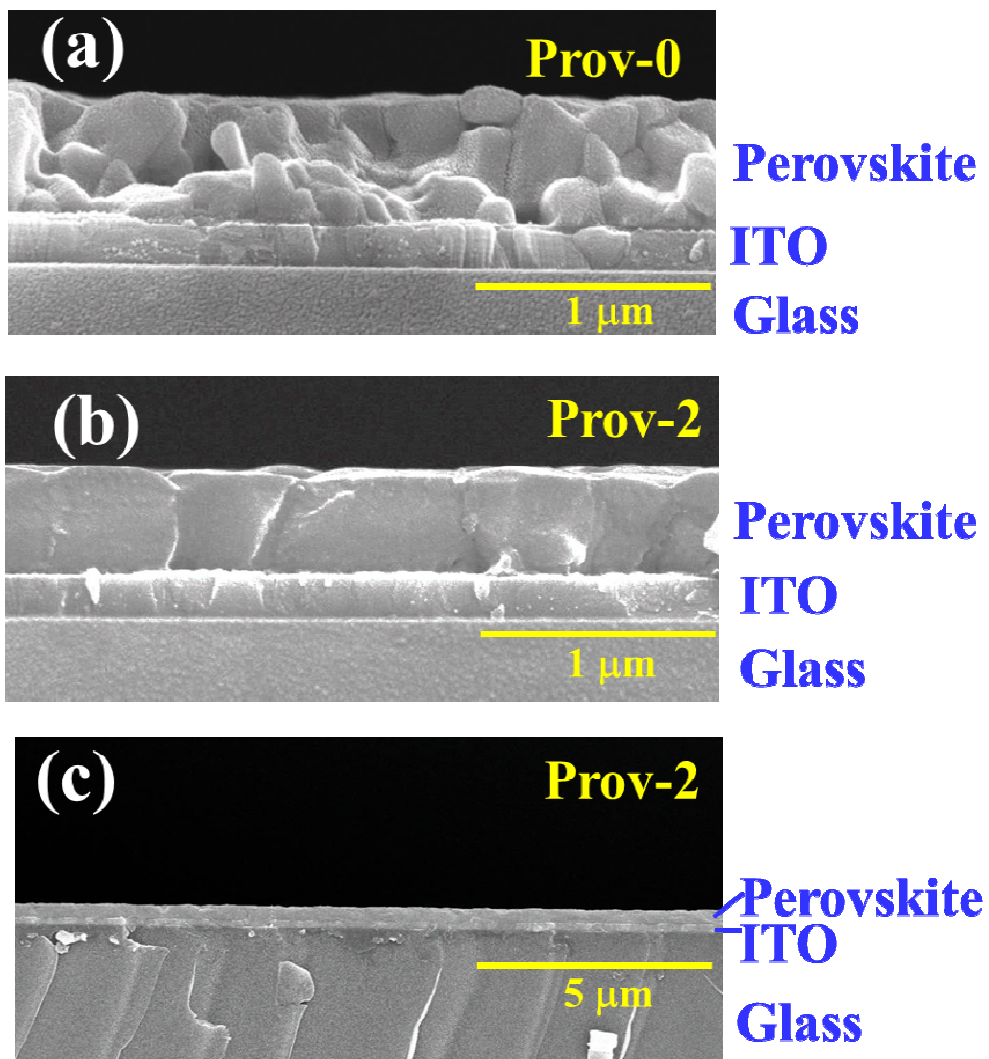


Figure 8

